Macromolecular Bioscience
www.mbs-journal.de

Let There Be Light: Targeted Photodynamic Therapy Using High Aspect Ratio Plant Viral Nanoparticles

*Paul L. Chariou, Lu Wang, Cian Desai, Jooneon Park, Leanna K. Robbins, Horst A. von Recum, Reza A. Ghiladi, and Nicole F. Steinmetz**

The development of plant viral nanoparticles (VNP) loaded with different molecular versions of a photodynamic drug is described. Specifically, tobacco mosaic virus (TMV) and tobacco mild green mosaic virus (TMGMV) are developed as drug carriers that encapsulate the monocationic, dicationic, tricationic, and tetracationic versions of a porphyrin-based photosensitizer drug (Zn-Por). While TMV has been extensively explored for various nanotechnology applications, this is the first study investigating TMGMV for medical applications. Light-activated cancer cell killing of Zn-Por-loaded VNPs is studied in vitro using melanoma and cervical cancer models. Native and nucleolin-targeted VNP drug carriers are developed and their efficacy assessed. A fivefold increase in cancer cell killing is observed using nucleolin-targeted TMV loaded with tricationic Zn-Por and displaying the nucleolin-specific F3 peptide.

Photodynamic therapy (PDT) has emerged as an efficacious adjuvant treatment modality for several types of cancer.[1] In PDT, light is used to locally excite a photosensitizer (PS) to generate reactive oxygen species. The resulting oxidative stress disrupts organelle functions, promotes cell apoptosis, and damages the tumor vasculature that supplies oxygen and nutrients required for the tumor to survive.[2] While a few PDT therapies have received Food and Drug Administration (FDA) approval (i.e., Photofrin and aminolevulinic acid), efficient delivery of the PS to the target site remains challenging. Tumor accumulation of the PS is generally poor due to the physicochemical properties of the PS.[3] Therefore, large doses are administered to compensate for the poor drug accumulation at the target site. This is particularly unfavorable because most PSs suffer from slow in vivo clearance, which increases toxicity. For example, as skin is highly vascularized and easily exposed to light, the long circulation time of PS (e.g., Photofrin[4] has a half-life of 452 h) promotes skin phototoxicity. As a result, patients are required to limit their exposure to the sun several weeks post-treatment. Therefore, there is a critical need to develop delivery systems with enhanced clearance that promote the accumulation of the PS in the tumor site.

To this end, we turned toward the development of plant virus-based nanoparticles (VNPs) for the delivery of PS. VNPs have been developed as carriers for the delivery of contrast agents, chemotherapeutics, protein therapies, epitopes, agropesticides, as well as PS.[5–9] Plant VNPs have several attributes that are favorable for nanomedicine delivery and in particular PS delivery. Bio-manufacturing is well established and the biologic platform offers well-defined, monodisperse structures that can be tailored with molecular precision.[7] Plant VNPs are non-infectious toward mammals, and most importantly the proteinaceous nanoparticles are cleared rapidly from circulation and from tissue,[10,11] thus making this a particularly attractive platform for PS delivery. Plant VNPs as well as bacteriophage-derived nanoparticles have been developed for PS delivery[7]; in most instances, PS agents are covalently coupled to viral carriers. However, covalent binding of the PS to nanoparticles may impair their photoactivity due to quenching and reduced molecular freedom, and in turn limit their intracellular activity. Therefore, non-covalent drug delivery may be advantageous to enhance and control steady release of the PS within the tumor environment. This strategy relies on hydrophobic-hydrophilic and electron charge interactions between the PS and its carrier.

In this work, we utilized two high aspect ratio, soft matter tubular nanostructures for PS delivery, namely tobacco mosaic

P. L. Chariou, L. Wang, Dr. J. Park, Prof. N. F. Steinmetz
Department of BioEngineering
University of California San Diego
La Jolla, CA 92039, USA
E-mail: nsteinmetz@ucsd.edu
Prof. N. F. Steinmetz
Department of NanoEngineering
University of California San Diego
La Jolla, CA 92039, USA
Prof. N. F. Steinmetz
Moores Cancer Center
University of California San Diego
La Jolla, CA 92039, USA
Prof. N. F. Steinmetz
Department of Radiology
University of California San Diego
La Jolla, CA 92039, USA
P. L. Chariou, L. Wang, C. Desai, Dr. J. Park, Prof. H. A. von Recum, Prof. N. F. Steinmetz
Department of Biomedical Engineering
Case Western Reserve University
Cleveland, OH 44106, USA
Dr. L. K. Robbins, Prof. R. A. Ghiladi
Department of Chemistry
North Carolina State University
Raleigh, NC 27695, USA
The ORCID identification number(s) for the author(s) of this article can be found under https://doi.org/10.1002/mabi.201800407.

DOI: 10.1002/mabi.201800407

virus (TMV) and tobacco mild green mosaic virus (TMGMV). TMV and TMGMV were selected as carrier platforms based on their well-established surface chemistry and elongated shape. Elongated (rod-shaped or filamentous) nanoparticles have enhanced blood margination, transport across tissue membrane, cell adherence, and macrophage avoidance, promoting their accumulation in the tumor tissue.[12,13] TMV and TMGMV self-assemble helically around a single-stranded RNA genome to form a 300 × 18 nm rod with a 4 nm-wide hollow interior channel (**Figure 1**A). Both particles are made of 2130 identical copies of coat protein units; TMV and TMGMV share 86% sequence homology.[14] Of particular interest, the interior channels of TMV and TMGMV are covered with solvent-exposed glutamic acids that are readily available for electrostatic loading of positively charged guest molecules (Figure 1A).[14] While TMV has been extensively studied for clinical applications, including the delivery of PS,[5] this is the first study investigating TMGMV for medical applications. To probe drug loading and release, we studied the monocationic, dicationic, tricationic, and tetracationic version of a zinc porphyrin photosensitizer. Last, we selected one formulation and developed a cancer cell targeting strategy to further enhance treatment efficacy.

Monocationic (Zn-Por^{1+}), dicationic (Zn-Por^{2+}), tricationic (Zn-Por^{3+}), and tetracationic (Zn-Por^{4+}) drugs were synthesized using previously established protocols[15] and the appropriate starting aldehydes (Figure S1, Supporting Information). Zn-Por$^{1+,2+,3+,4+}$ were incubated with TMV and TMGMV using a molar excess of 500:1, 2000:1, 5000:1, 10 000:1 Zn-Por:VNP in 10 mM potassium phosphate (KP) buffer (pH 7.8) overnight at room temperature with gentle agitation (Figure 1A). The mixture was then purified by ultracentrifugation at 112 000 × *g* for 1 h on a 30% w/v sucrose cushion to separate the Zn-Por-loaded particles ($VNP_{Zn\text{-}Por}$) from the excess Zn-Por molecules. The resulting pellet was resuspended in 10 mM KP (pH 7.8) overnight and centrifuged at 16 000 × *g* for 10 min to remove potential aggregates. Finally, $VNP_{Zn\text{-}Por}$ were eluted through PD Minitrap G-25 desalting columns to entrap any remaining unbounded Zn-Por. The purified reaction mixtures were analyzed by UV–vis to quantify drug loading using the extinction coefficient of Zn-Por (195 000 $M^{-1} \cdot cm^{-1}$) at 440 nm (Figure 1B,C).

The maximum drug loading, yielding ≈600–700 Zn-Por molecules per VNP, was obtained using a 2000 molar excess of Zn-Por. Increased molar excess did not yield increased drug loading, but rather resulted in a loss of particle recovery due to the increased formation of aggregates (Figure S2A,B, Supporting Information). For TMGMV, charge appeared to have little effect on loading efficiency—independent of molecular Zn-Por version used, >500 Zn-Por molecules were incorporated into TMGMV. In stark contrast, the charge of the different Zn-Por formulations greatly influenced their loading efficiency in TMV: Zn-Por^{1+} (≈180 molecules/TMV), Zn-Por^{2+} (≈250 molecules/TMV), and Zn-Por^{4+} (≈400 molecules/TMV) all resulted in lower loading efficiency versus ≈600 molecules per TMV for Zn-Por^{3+}, the latter is comparable to previously obtained data.[5]

The TMV results can be attributed to the combined effect of electrostatic and hydrophobic/hydrophilic interactions; the greater the positive charge, the better stabilization inside the TMV interior channel. In addition, the increased hydrophobic

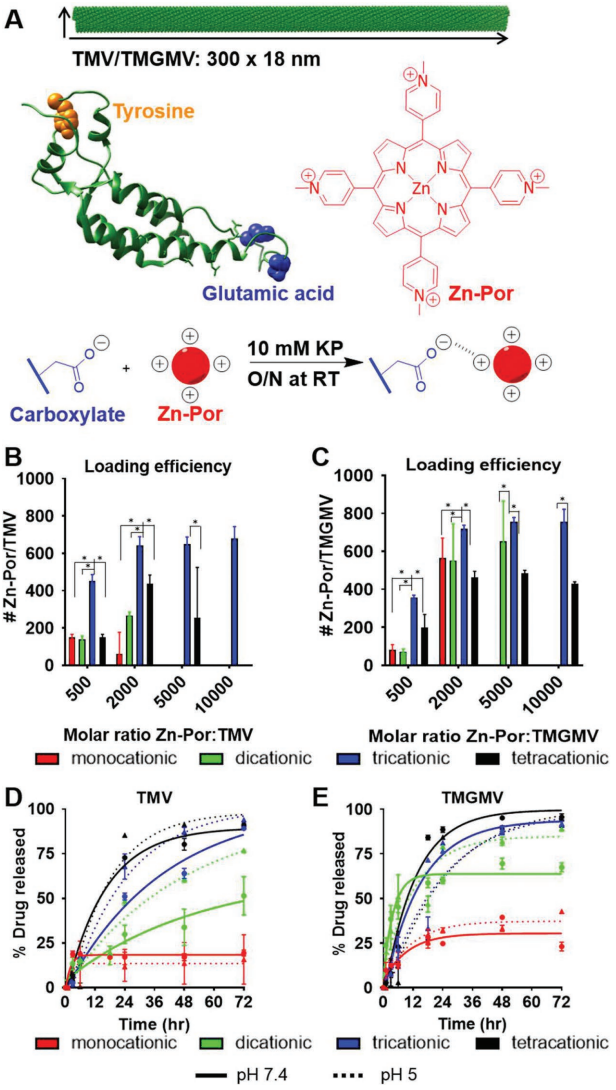

Figure 1. Evaluation of Zn-Por loading and release from TMV and TMGMV. A) The full length structure of TMV/TMGMV is made of 2130 identical coat proteins. A single coat protein is depicted highlighting the exterior surface exposed tyrosine (orange) and the interior surface exposed glutamic acids (blue). The chemical structure of the cationic Zn-Por (red) is shown to the right of the coat protein. The tetracationic (4 positive charges) Zn-Por was here selected as an example. When the virus and Zn-Por are mixed together at pH 7.8, the cationic Zn-Por and the deprotonated carboxylate residue of glutamic acid form an electrostatic bond. B) Average number of each Zn-Por formulation in TMV and C) TMGMV as a function of the starting Zn-Por:VNP molar ratio. Statistical significance was established using an Anova test with $p < 0.01$. D) Cumulative Zn-Por release profile from TMV and E) TMGMV at physiological pH 7.4 (solid line) and endosomal/tumor environment pH 5 (dashed line).

nature of the monocationic and dicationic Zn-Por formulations in combination with their electrostatic properties led to the formation of more aggregates compared to their tricationic and tetracationic counterparts, thereby reducing the loading efficiency. Several factors may explain the differential loading results between TMGMV and TMV. We have previously compared the amino acid sequences of TMV and TMGMV and analyzed their

distribution of charged residues on both the inner and outer surfaces of the virus.[14] While it has been shown that only two glutamic acid (Glu) residues are chemically available on TMV (Glu 97 and Glu 106), our analysis revealed that in addition to the Glu 95 and Glu 106 in the interior channel of TMGMV, Glu 145 and aspartic acid (Asp) 66 were also exposed on the outer surface and could be available for electrostatic charge interactions. The difference in the amino acid sequences of TMV and TMGMV could also play a role in the difference in loading by changing the charge and hydrophobicity surrounding the glutamic acid residues. Furthermore, the virus coat proteins are not rigid structures, and therefore small molecules could diffuse in between coat proteins. It is conceivable that TMGMV has greater coat protein fluidity and therefore a higher loading capacity.

Based on the above studies, we prepared drug-loaded VNPs using the 2000:1 Zn-Por:VNP ratio. We studied whether changing the pH of the 10 mM KP buffer solution would influence the loading efficiency of Zn-Por into TMV and TMGMV (Figure S2C–F, Supporting Information). At pH 3, VNPs aggregated and disassembled, which led to lower yields. The corresponding loading efficiency was low due to the protonation of carboxylate groups, resulting in weak electrostatic interaction. At pH 5, the reaction yields and loading efficiency were improved compared to pH 3, and reached their maximum at pH 7.8. Increasing the pH to 10 did not increase the loading yield, but rather just slightly decreased loading efficiency and reaction yields. While ≈60–75% of starting materials were recovered at pH 7.8, the yield dropped to ≈40% at pH 10. Based on the findings of the pH studies, we conducted the remaining experiments at pH 7.8 due to the relatively high loading efficiency and recovery observed at this pH.

Next, we analyzed the drug release profile of each Zn-Por:VNP formulation (Figure 1D,E). One milligram of particles was resuspended in 300 µL PBS and loaded in triplicate in 10 000 MW cut-off Slide-A-Lyzer MINI dialysis units for 72 h. To mimic physiological conditions, samples were dialyzed against 3 L of PBS adjusted to pH 7.4 (physiologic conditions, e.g., blood pH) as well as pH 5 (acidic conditions, e.g., acidic tumor microenvironment or endolysosomal pH) at 37 °C. At time $t = 0$, 1, 3, 6, 18, 24, 48, and 72 h, 10 µL was extracted from each dialysis unit and the remaining Zn-Por entrapment was measured by UV–vis spectroscopy. The half-life $t_{1/2}$, defined as the time required for 50% of the drug to be released from the VNPs, decreases as the electropositivity of Zn-Por increases. At pH 7.4, TMV: Zn-Por^{4+} and TMGMV: Zn-Por^{4+} formulations had the lowest $t_{1/2}$ (12 and 10 h, respectively). In contrast, only 20% and 25% of Zn-Por^{1+} was released from TMV and TMGMV respectively within 72 h. The release profiles of Zn-Por^{3+} were similar to that of Zn-Por^{4+}, while the release rates of Zn-Por^{2+} were in between those of Zn-$Por^{4+/3+}$ and Zn-Por^{1+}. While the $t_{1/2}$ values of each Zn-Por:VNP formulation were slightly lower at pH 5, the trend remained the same. These results indicate that the dominant force of interaction between TMV/TMGMV and Zn-Por is not electrostatic, but rather hydrophobic/hydrophilic. Since Zn-Por becomes more hydrophobic as its electropositivity is reduced, its ability to solubilize in PBS surrounding the VNP is impaired, thereby decreasing the rate of drug release. We also tested stability of the Zn-Por:VNP formulations under storage conditions (i.e., 10 mM KP, pH 7.8, 4 °C), and observed a slow and constant release of Zn-Por from TMV and TMGMV over a period of 6 weeks (Figure S2G,H, Supporting Information). The release rate of Zn-Por in storage conditions was ranked from highest to lowest. For TMV, Zn-Por^{1+} > Zn-Por^{2+} = Zn-Por^{3+} > Zn-Por^{4+}, whereas TMGMV showed a different trend: Zn-Por^{2+} = Zn-Por^{3+} > Zn-Por^{1+} > Zn-Por^{4+}. Specifically, 50% of Zn-Por was released from TMV:Zn-Por^{1+} (the lowest loading efficiency ≈180) and TMGMV: Zn-$Por^{2+/3+}$ within 25–28 days. Less than 45% of Zn-Por was released from the other formulation within 6 weeks.

To evaluate in vitro efficacy of Zn-Por:VNP formulations, we first compared TMV and TMGMV's uptake by B16F10 melanoma cells. Melanoma was chosen as a model because PDT has shown promise in melanoma.[5] While most melanomas are removed by surgery supplemented with adjuvant chemotherapy and/or immunotherapy, some melanomas remain unresponsive to these therapies. A growing body of data indicates that PDT could be applied as an adjuvant therapy for those melanomas not responsive to traditional therapies.[16]

For cell uptake studies, TMV and TMGMV were conjugated with the fluorophore Cyanine 5 (Cy5) using solvent exposed tyrosine side chains (on the exterior TMV/TMGMV surface, Figure 1A) click chemistry,[14] followed by the purification of the reaction mixture as previously described. The covalent attachment of Cy5 was confirmed by UV–vis and denaturing SDS-NuPAGE gel electrophoresis (Figure S3A, Supporting Information). We have previously demonstrated that a minimum conjugation of Cy5 to ≈8% of TMV coat proteins (CPs) is sufficient to yield maximum fluorescence intensity.[17] TMV and TMGMV particles displayed ≈160 (7.5%) and ≈490 (23%) dyes respectively. The higher dye conjugation efficiency in TMGMV could be due to differences in the chemical microenvironment (i.e., surrounding amino acids with different charge and hydrophobicity) and greater surface exposure of the tyrosine side chain. The corresponding average distances between fluorophores are equal to 2.7 and 1.6 nm for TMV and TMGMV, respectively, which are large enough to prevent quenching due to energy transfer between dye molecules and trapping by dimers.[17] Therefore, these Cy5-TMV and Cy5-TMGMV constructs are suitable for imaging experiments.

To assess VNP–cell interactions, B16F10 melanoma cells were incubated with 100 000 VNPs per cell at 37 °C and 5% CO_2 for 1 and 8 h in Dulbecco's modified Eagle's media (DMEM) supplemented with 10% v/v fetal bovine serum and 1% w/v penicillin-streptomycin. Cells were washed thoroughly with FACS buffer (0.2% v/v 0.5 M EDTA, 1% v/v FBS and 2.5% v/v 1 M HEPES pH 7.0 in DPBS) and fixed with 2% v/v paraformaldehyde. Cells were then analyzed using a BD Accuri C6 Plus flow cytometer and 1×10^4 events were recorded. Data were analyzed using FlowJo v8.6.3 software. After 1 h of incubation, 85% and 100% of TMV and TMGMV were taken up by B16F10 cells, respectively (**Figure 2**A). This is reflected by an increase in mean fluorescence intensity compared to cells only (Figure 2B). The slightly higher uptake of TMGMV may be attributed to greater particle instability during viral production and purification, which causes some of the particles to be broken[14]; a shorter TMGMV rod would have a faster rate of cell penetration. Nonetheless, the cellular uptake of TMV

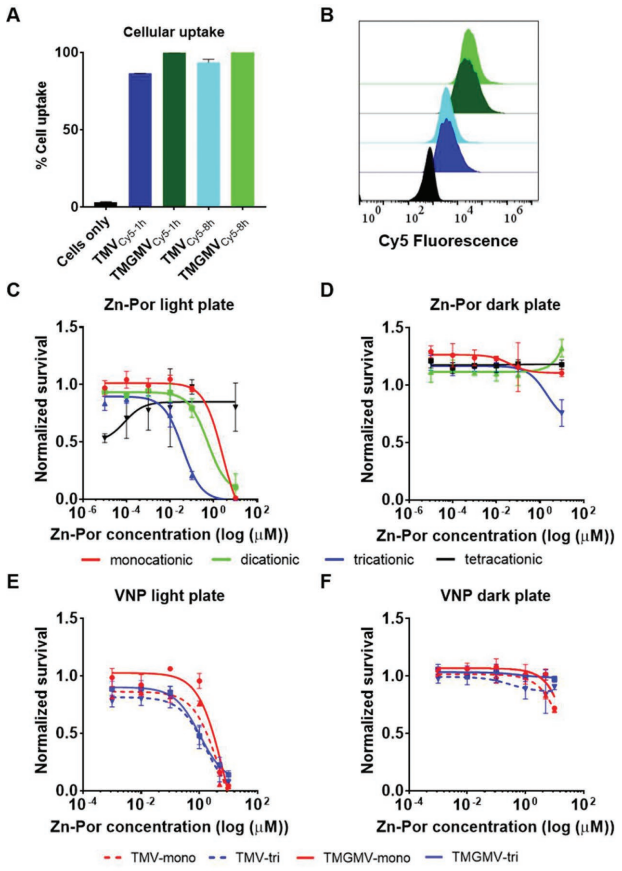

Drug	IC_{50} (μM)	Drug:VNP	IC_{50} (μM)
Zn-Por1+	2.5	Zn-Por1+:TMV	4.7
Zn-Por2+	0.5	Zn-Por3+:TMV	1.5
Zn-Por3+	0.03	Zn-Por1+:TMGMV	7
Zn-Por4+	NA	Zn-Por3+:TMGMV	1

Figure 2. In vitro treatment of B16F10 cells. A) Flow cytometry quantification of the percent cellular uptake of Cy5-TMV and Cy5-TMGMV in B16F10 melanoma cells after 1 and 8 h of incubation. B) Corresponding fluorescent intensity reading. C) B16F10 melanoma cell viability (MTT assay) following 8 h incubation with increasing doses of Zn-Por and 30 min illumination with white light. D) The corresponding cell viability in the absence of light treatment. The treatment was repeated using selected Zn-Por:VNP formulations E) with and F) without light treatment.

and TMGMV reached 93% and 100%, respectively, after 8 h of incubation. This time point was selected to allow VNPs to internalize before proceeding with the photodynamic treatment.

We evaluated efficacy of the drug delivery approach against B16F10 cells using previously established white light therapy.[5] The following samples were tested: Drug-free VNPs, free Zn-Por, and Zn-Por-loaded VNPs, and a dark control for each sample was included. Cells were incubated with 0.001, 0.01, 0.1, 1, 5, and 10 μM of Zn-Por, Zn-Por:VNP, or controls for 8 h at 37 °C and 5% CO_2. Cells were washed to remove any Zn-Por that was not endocytosed and samples were illuminated under white light (10 mW cm^{-2} at 430 nm) for 30 min (18.1 J cm^{-2} at 430 nm). Control samples were kept in the dark at 37 °C and 5% CO_2. In all experiments, neither dark controls (Figure 2D and F) nor any of the VNP-only controls (not shown) showed significant cell toxicity. After illumination, plates were incubated for an additional 48 h and cell viability was assessed using the MTT cell proliferation assay according to the manufacturer's recommended protocol. The IC_{50} values of free Zn-Por^{1+}, Zn-Por^{2+}, and Zn-Por^{3+} were 2.5, 0.5, and 0.03 μM, respectively. The tetracationic Zn-Por showed little to no cell toxicity. Based on these results, we selected Zn-Por^{1+} and Zn-Por^{3+} and proceeded to repeat the experiment with the corresponding Zn-Por:VNP formulations. Zn-Por^{1+}:TMV, Zn-Por^{3+}:TMV, Zn-Por^{1+}:TMGMV, and Zn-Por^{3+}:TMGMV displayed IC_{50} equal to 4.7, 1.5, 7, and 1 μM, respectively.

Free Zn-Por^{1+} was 1.8 to 2.8-fold more effective compared to its TMV/TMGMV formulation; this reduced efficacy was even more dramatic for the Zn-Por^{3+} loaded particles which showed a 30–50-fold decrease in efficacy. The decreased drug activity of VNPs loaded with Zn-Por versus free Zn-Por is expected. The reactive oxygen species produced by PS drugs have a very short half-life and act locally from their generation site. Therefore, the subcellular localization of the PS greatly influences its phototoxicity. Like most nanoparticles, TMV and TMGMV are internalized by endocytosis and follow the endosomal-lysosomal pathway. Previous data suggest the phototoxicity of PS localized in lysosomes is significantly reduced compared to PS localized in other organelles, in particular in mitochondria.[18] On the other hand, hydrophobic PS with cationic charges such as free Zn-Por is likely to localize in mitochondria.[18] Nonetheless, TMV and TMGMV are here used to improve the bioavailability and tumor accumulation of Zn-Por while reducing non-specific tissue toxicity. TMV and TMGMV can be further chemically or genetically modified to display moieties such as cancer cell targeting ligands, cell penetrating ligands, and chemotherapeutics for combined therapy, which would further improve the treatment efficacy.

As a proof of concept, we set out to develop a targeted Zn-Por delivery system. We chose Zn-Por^{3+} and TMV, in particular we used the well-established and characterized Lys-added mutant denoted as TMV_{lys}.[19] While TMGMV showed greater toxicity than TMGMV, the genetic engineering of $TMGMV_{lys}$ mutant has yet to be established in the future. TMV_{lys} offers amine functional groups for bioconjugation: targeting ligands synthesized with a terminal Cys side chain can be conjugated using heterobifunctional NHS-maleimide linkers. Here we chose the F3 peptide (KDEPQRRSARLSAKPAPPKPEPKPKKAPAKK) as the ligand.[20] The F3 peptide is a 31-amino acid fragment of the high mobility group protein HMG2N. F3 preferentially binds to nucleolin, a shuttle protein that is highly expressed on the plasma membranes of tumor cells.[21,22] Nucleolin-targeted delivery of drug-loaded nanoparticles using F3 peptide or nucleolin-specific aptamers has been previously demonstrated.[23–25] For example, F3-functionalized PEG-PLA nanoparticles led to deeper tumor penetration into 3D glioma spheroids and prolonged the survival of mouse bearing intracranial C6 glioma when loaded with paclitaxel.[25] In this work, we conjugated F3 to TMV_{lys} following an established protocol (**Figure 3**A).[26] In

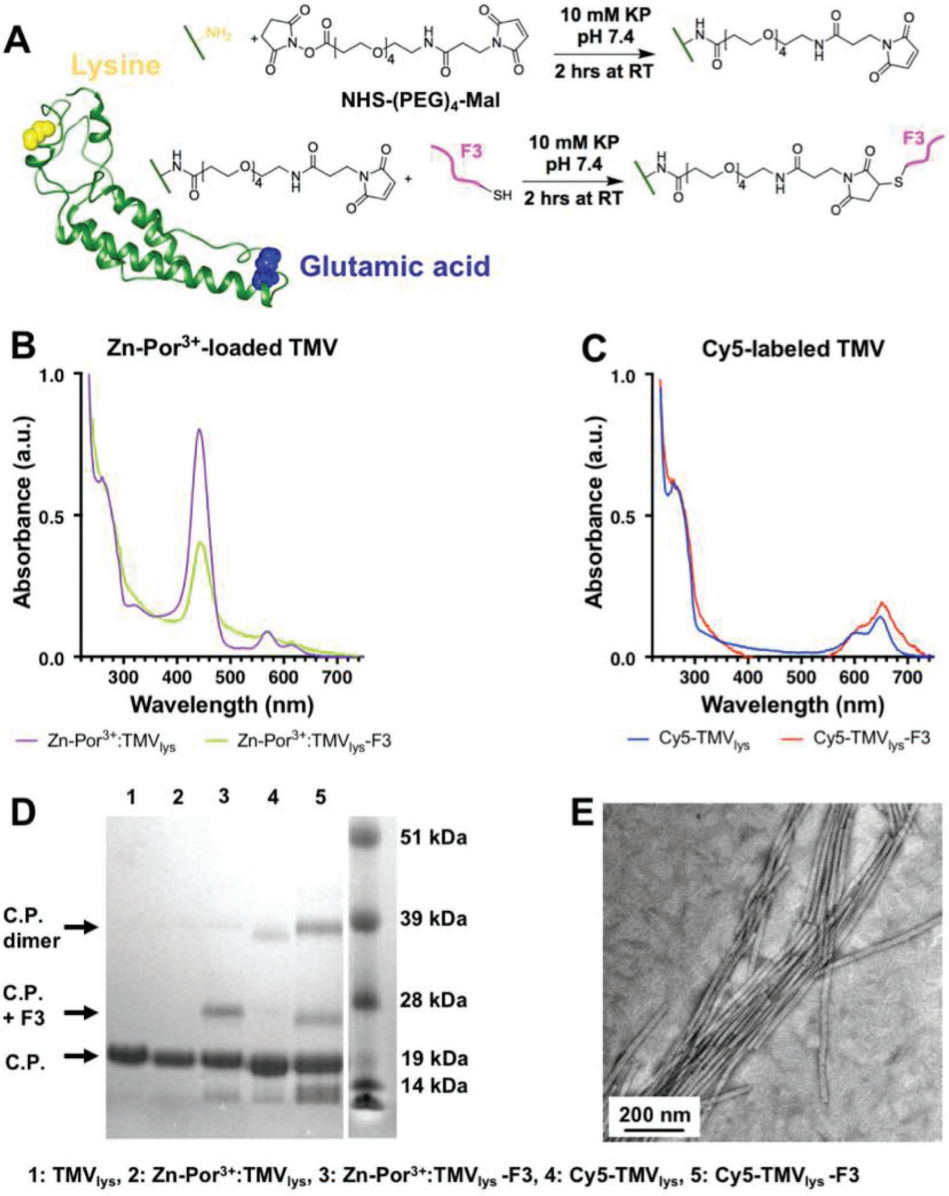

Figure 3. Synthesis of targeted TMV_{lys}-F3 particles. A) Two-step conjugation scheme. A single TMV_{lys} coat protein is depicted on the left, with surface-exposed lysine (yellow) and glutamic acids (blue). The F3 peptide with C-terminal cysteine is conjugated to the exterior lysine residues of TMV_{lys} using a bifunctional PEG linker. B) UV–vis spectra of Zn-Por^{3+}-loaded and C) Cy5-labelled TMV_{lys} and TMV_{lys}-F3, with characteristic A_{260}:A_{280} ratio for intact TMV_{lys}; note the absorption maxima at λ_{440} for Zn-Por^{3+} and λ_{649} for Cy5. D) SDS-PAGE gel image of TMV_{lys} particles, with positions for bare and conjugated coat proteins highlighted. E) TEM image of Cy5-TMV_{lys}-F3.

brief, TMV_{lys} was mixed with a maleimide-PEG_4-NHS bifunctional linker using 10 equivalents linker per TMV_{lys} coat protein in 10 mM KP buffer (pH 7.4) for 2 h. The mixture was then purified by ultracentrifugation at 112 000 × *g* for 1 h on a 40% w/v sucrose cushion. The F3 peptide synthesized with a C-terminal Cys (GenScript) was then added to the mixture at 0.5 equivalents peptide per TMV_{lys} coat protein and reacted for 2 h. The final TMV_{lys}-F3 was purified with 10 000 MW cut-off Slide-A-Lyzer MINI dialysis units. A higher excess of the F3 peptides led to aggregation and a lower excess did not show sufficient conjugation yields. Cy5-labelled TMV_{lys}-F3 was also prepared for cell uptake studies. Cy5 fluorophore conjugation was carried as described above prior to F3 conjugation. Using the aforementioned protocol, SDS-NuPAGE gel electrophoresis confirmed covalent attachment of F3 peptides, as indicated by higher molecular-weight bands (Figure 3D) The TMV coat protein has a molecular weight of ≈17.5 kDa; a slightly higher molecular weight indicates the addition of F3 peptide (≈4.2 kDa). ImageJ software was used to quantify the degree of F3 conjugation, and the data indicate that over 20% of the TMV_{lys} coat proteins were modified with F3 peptide. The A_{260}:A_{280} ratios (RNA:protein) of Cy5-TMV_{lys}-F3 and Zn-Por:TMV_{lys}-F3 were 1.21 and 1.29, respectively, which are indicative of intact TMV preparations

(Figure 3B,C). Furthermore, transmission electron microscopy (TEM) indicated that TMV_{lys} maintained its structural integrity post chemical modifications (Figure 3E).

To assess the targeting efficacy, we compared the cellular uptake of Cy5-labeled TMV_{lys} and TMV_{lys}-F3 particles using HeLa cells. HeLa cells were chosen because this cervical cancer cell line is known to express high levels of nucleolin.[21,27] For cell targeting studies, HeLa cells were incubated with 150 000, 300 000, or 750 000 particles per cell at 37 °C and 5% CO_2 for 3 h in DMEM supplemented with 10% v/v fetal bovine serum and 1% w/v penicillin-streptomycin. Flow cytometry was performed as described above. Flow cytometry showed an over 50% increase in cell uptake of conjugated Cy5-TMV_{lys}-F3 particles (**Figure 4**A). Compared to cells incubated with native TMV particles, the mean fluorescence intensity increased by 40-fold in the presence of nucleolin-targeted Cy5-TMV_{lys}-F3 particles (Figure 4B,C). Because the flow cytometry does not provide insights into the fates of the nanoparticles, we also used confocal microscopy to study where the particles localized within the cells. HeLa cells were incubated with 6 000 000 particles per cell for 6 h in culture medium. Then cell membranes were stained with Alexa Fluor 555-conjugated wheat germ agglutinin (1:500 dilution) and mounted with Fluoroshield with DAPI. Slides were imaged using a Leica TCS SPE confocal laser scanning microscope and the data were analyzed using ImageJ software. The confocal images were in agreement with flow cytometry, showing high cell interactions of the F3-targeted TMV formulation. The Cy5-TMV_{lys}-F3 particles appear bundled up on the surface of HeLa cells, where nucleolin is overexpressed (Figure 4E). Although others have shown intracellular trafficking of F3-functionalized polymeric nanoparticles,[28] cellular uptake of Cy5-TMV_{lys}-F3 was not observed in our study. This possibly indicates that the TMV's high aspect ratio shape may not be suitable to be shuttled by nucleolin. Nevertheless, the accumulation of Cy5-TMV_{lys}-F3 particles on the cell membrane may be advantageous for PDT as cell membrane targeting may prevent trapping of zinc porphyrin in endolysosomes and therefore enhance its cytotoxic efficacy. We moved on to explore the therapeutic efficacy of the F3-targeted Zn-Por drug delivery system.

The enhanced cytotoxic efficacy of Zn-Por^{3+} loaded in TMV_{lys}-F3 was reflected in the decreased survival of HeLa cells after white light treatment (Figure 4F). TMV_{lys} particles were loaded with 2000:1 molar excess of Zn-Por^{3+} as described above prior to the conjugation of F3 peptides. From the MTT cell proliferation assay, the IC_{50} values for Zn-Por^{3+} in HeLa cells were equal to 0.034, 0.38 and 0.19 μM for Zn-Por^{3+}-TMV_{lys}-F3, Zn-Por^{3+}-TMV_{lys}, and free Zn-Por^{3+} respectively. No cell killing was observed with drug-free TMV_{lys}-F3 particles at maximum concentration. Without light treatment, data indicated that Zn-Por^{3+}-TMV_{lys}-F3 is non-toxic to HeLa cells (Figure S4, Supporting Information). Compared to the data reported above, the efficacy of free Zn-Por^{3+} drug with white light treatment was sixfold higher in B16F10 cells than in HeLa cells. This may be attributed to the biochemical differences between a mouse cell line and a human cell line. The drug activity decreased by half after loading into TMV_{lys}-F3. This level of activity decrease after loading was not as significant as our previous data with TMV and TMGMV particles in B16F10 cells, yet the trend of decreased activity after loading into VNP did agree. Meanwhile,

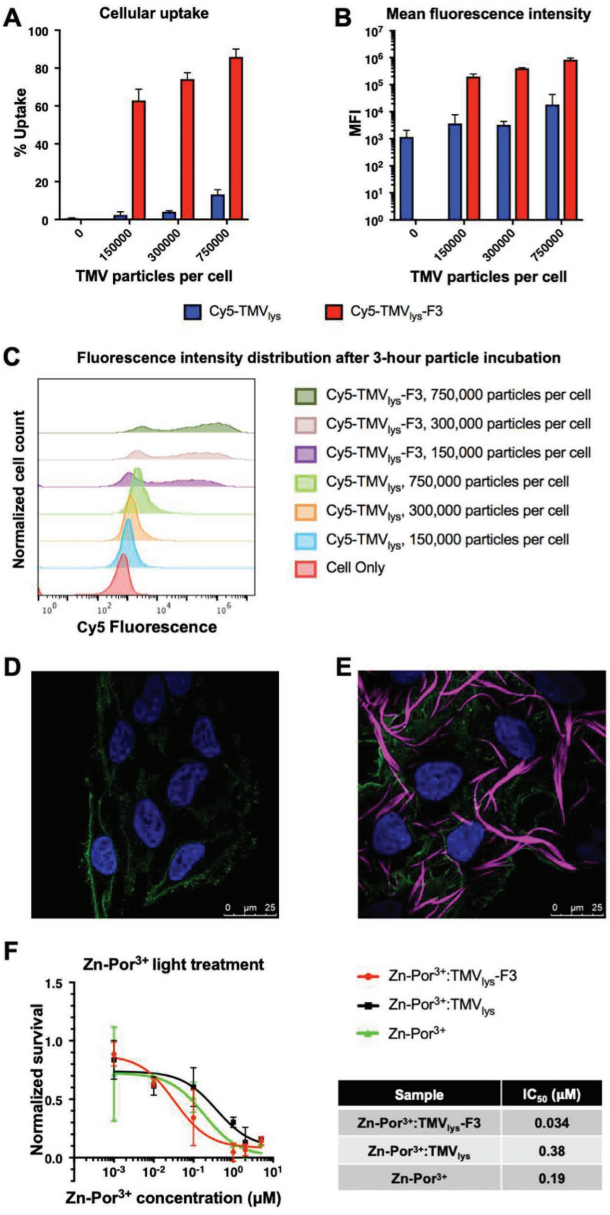

Figure 4. Uptake of TMV_{lys}-F3 particles by HeLa cells in vitro. Flow cytometry results showing A) the percent cellular uptake, B) mean fluorescence intensity, and C) corresponding fluorescence spectra of HeLa cells incubated with Cy5-labeled TMV with and without F3 ligand. D) Confocal fluorescence microscopy image of HeLa cells stained showing DAPI (blue), AF555 conjugated wheat germ agglutinin (green) and Cy5 (magenta) after 6-h incubation with Cy5-TMV_{lys} and E) with Cy5-TMV_{lys}-F3. F) HeLa cell viability (MTT assay) following 8-h incubation with increasing doses of Zn-Por and Zn-Por loaded TMV with and without F3 ligand following 30 min illumination with white light.

the targeted Zn-Por^{3+}-TMV_{lys}-F3 particles showed a fivefold increase in cell killing efficacy compared to the free drug. The increase PDT activity of Zn-Por^{3+}-TMV_{lys}-F3 versus Zn-Por^{3+}-TMV_{lys} may be explained as follows: i) a significantly larger amount of particles targets cancer cells when using TMV_{lys}-F3 versus its native counterpart; and ii) TMV_{lys}-F3 targets the cell membrane; light activation may lead to cell toxicity through cell

membrane disruption, and iii) it is also possible that the PS cargo is released at the cell surface, and since the Zn-Por molecule is cell permeable and positively charged, cell uptake maybe favored—in contrast, TMV without the F3 ligand accumulates in the endolysosomal compartment.

In summary, we have successfully investigated the loading and release profiles of Zn-Por into both TMV and TMGMV as a function of ionic state or charge of Zn-Por. We have shown that free Zn-Por^{3+} had the greatest cell toxicity and loading of Zn-Por into TMV and TMGMV resulted in a slightly decreased cell toxicity in vitro. Critically, our studies suggest that nucleolin-targeted VNP formulations carrying the Zn-Por^{3+} PS has greatest anti-cancer efficacy. The F3 nucleolin targeting ligand increases nanoparticle and therefore drug accumulation; at the same time the cellular distribution is altered with F3-targeted TMV accumulating at the cancer cell surface. Such targeted nanotechnologies hold great potential for cancer therapies with higher specificity increasing the patient's quality of life, but most importantly survival.

Supporting Information

Supporting Information is available from the Wiley Online Library or from the author.

Acknowledgements

This work was supported by a grant from the National Science Foundation CAREER DMR 1452257 (to N.F.S.) and a Biotechnology Innovation Grant (2016-BIG-6537) from the North Carolina Biotechnology Center (to R.A.G.).

Conflict of Interest

The authors declare no conflict of interest.

Keywords

cancer phototherapy, nucleolin targeting, tobacco green mosaic virus, tobacco mosaic virus, zinc photosensitizer

Received: October 20, 2018
Revised: December 7, 2018
Published online:

[1] P. Agostinis, K. Berg, K. A. Cengel, T. H. Foster, A. W. Girotti, S. O. Gollnick, S. M. Hahn, M. R. Hamblin, A. Juzeniene, D. Kessel, M. Korbelik, J. Moan, P. Mroz, D. Nowis, J. Piette, B. C. Wilson, J. Golab, *Ca-Cancer J. Clin.* **2011**, *61*, 250.
[2] D. W. Felsher, *Nat. Rev. Cancer* **2003**, *3*, 375.
[3] W. Wang, L. T. Moriyama, V. S. Bagnato, *Laser Phys. Lett.* **2013**, *10*, 023001.
[4] M. J. Alonso, M. Garcia-Fuentes, *Nano-Oncologicals: New Targeting and Delivery Approaches*, Springer, Berlin **2014**.
[5] K. L. Lee, B. L. Carpenter, A. M. Wen, R. A. Ghiladi, N. F. Steinmetz, *ACS Biomater. Sci. Eng.* **2016**, *2*, 838.
[6] M. Brasch, A. de la Escosura, Y. Ma, C. Uetrecht, A. J. R. Heck, T. Torres, J. J. L. M. Cornelissen, *J. Am. Chem. Soc.* **2011**, *133*, 6878.
[7] A. M. Wen, N. F. Steinmetz, *Chem. Soc. Rev.* **2016**, *45*, 4074.
[8] Y. Ma, R. J. M. Nolte, J. J. L. M. Cornelissen, *Adv. Drug Delivery Rev.* **2012**, *64*, 811.
[9] E. Alemzadeh, A. Dehshahri, K. Izadpanah, F. Ahmadi, *Colloids Surf., B* **2018**, *167*, 20.
[10] S. Shukla, A. M. Wen, N. R. Ayat, U. Commandeur, R. Gopalkrishnan, A. M. Broome, K. W. Lozada, R. A. Keri, N. F. Steinmetz, *Nanomedicine* **2014**, *9*, 221.
[11] S. Shukla, F. J. Eber, A. S. Nagarajan, N. A. DiFranco, N. Schmidt, A. M. Wen, S. Eiben, R. M. Twyman, C. Wege, N. F. Steinmetz, *Adv. Healthcare Mater.* **2015**, *4*, 874.
[12] S. Barua, S. Mitragotri, *Nano Today* **2014**, *9*, 223.
[13] N. P. Truong, M. R. Whittaker, C. W. Mak, T. P. Davis, *Expert Opin. Drug Delivery* **2015**, *12*, 129.
[14] P. L. Chariou, N. F. Steinmetz, *ACS Nano* **2017**, *11*, 4719.
[15] E. Feese, H. Sadeghifar, H. S. Gracz, D. S. Argyropoulos, R. A. Ghiladi, *Biomacromolecules* **2011**, *12*, 3528.
[16] B. Zhao, Y. Y. He, *Expert Rev. Anticancer Ther.* **2010**, *10*, 1797.
[17] A. M. Wen, M. Infusino, A. De Luca, D. L. Kernan, A. E. Czapar, G. Strangi, N. F. Steinmetz, *Bioconjugate Chem.* **2015**, *26*, 51.
[18] A. P. Castano, T. N. Demidova, M. R. Hamblin, *Photodiagn. Photodyn. Ther.* **2004**, *1*, 279.
[19] F. C. Geiger, F. J. Eber, S. Eiben, A. Mueller, H. Jeske, J. P. Spatz, C. Wege, *Nanoscale* **2013**, *5*, 3808.
[20] K. Porkka, P. Laakkonen, J. A. Hoffman, M. Bernasconi, E. Ruoslahti, *Proc. Natl. Acad. Sci. USA* **2002**, *99*, 7444.
[21] A. G. Hovanessian, C. Soundaramourty, D. E. Khoury, I. Nondier, J. Svab, B. Krust, *PLoS One* **2010**, *5*, e15787.
[22] Y. Huang, *Blood* **2006**, *107*, 3564.
[23] D. W. Hwang, H. Y. Ko, J. H. Lee, H. Kang, S. H. Ryu, I. C. Song, D. S. Lee, S. Kim, *J. Nucl. Med.* **2010**, *51*, 98.
[24] I. Winer, S. Wang, Y.-E. K. Lee, W. Fan, Y. Gong, D. Burgos-Ojeda, G. Spahlinger, R. Kopelman, R. J. Buckanovich, *Cancer Res.* **2010**, *70*, 8674.
[25] Q. Hu, G. Gu, Z. Liu, M. Jiang, T. Kang, D. Miao, Y. Tu, Z. Pang, Q. Song, L. Yao, H. Xia, H. Chen, X. Jiang, X. Gao, J. Chen, *Biomaterials* **2013**, *34*, 1135.
[26] N. M. Gulati, A. S. Pitek, N. F. Steinmetz, P. L. Stewart, *Nanoscale* **2017**, *9*, 3408.
[27] E. Grinstein, P. Wernet, P. J. F. Snijders, F. Rösl, I. Weinert, W. Jia, R. Kraft, C. Schewe, M. Schwabe, S. Hauptmann, M. Dietel, C. J. L. M. Meijer, H.-D. Royer, *J. Exp. Med.* **2002**, *196*, 1067.
[28] M. Qin, H. Zong, R. Kopelman, *Biomacromolecules* **2014**, *15*, 3728.